On sputter damage of silicon heterojunction solar cells and its recovery by illuminated annealing

© S.N. Abolmasov[1,2], V.S. Levitskii[1,2], A.S. Titov[1,2], E.I. Terukov[1,2]

[1] R&D Center of Thin Film Technologies in Energetics,
194064 St. Petersburg, Russia
[2] Ioffe Institute,
194021 St. Petersburg, Russia

E-mail: s.abolmasov@hevelsolar.com

Received March 3, 2025
Revised April 29, 2025
Accepted for publication May 5, 2025

Mechanisms of plasma damage caused by sputtering of transparent conductive oxide (TCO) layers in silicon heterojunction (SHJ) solar cells have been investigated. It is shown that a buffer layer at the amorphous/crystalline silicon (*a*-Si/*c*-Si) interface can play an essential role in mitigating the sputter damage. More than $9\,\%_{abs.}$ loss in the conversion efficiency is observed for rear emitter SHJ cells with nanocrystalline silicon *n*-layer when the underlying buffer layer changes from amorphous silicon carbide to amorphous silicon. It is revealed that the anomalous efficiency loss is mostly related to breaking Si-H bonds by NUV photons at the *a*-Si/*c*-Si interface during the TCO sputtering. Illuminated annealing of these cells at elevated temperature using a distributed light source based on light emitting diodes (LEDs) recovers the anomalous efficiency loss by more than $7\,\%_{abs.}$ Other possible mechanisms of sputter damage and mitigation strategies are also discussed.

Keywords: magnetron sputtering, transparent conductive oxide, *a*-Si/*c*-Si interface, surface passivation, conversion efficiency.

DOI: 10.61011/SC.2025.01.61076.7658

1. Introduction

Today silicon heterojunction (SHJ) solar cells hold the world record efficiency ($\eta \leq 27.6\,\%$ [1,2]) among single-junction silicon solar cells. This is mainly due to superior crystalline silicon (*c*-Si) surface passivation by thin hydrogenated amorphous silicon (*a*-Si:H) layers, resulting in the high open-circuit voltages (V_{OC}) measured on the record cells and low temperature coefficients [3,4]. The later along with their high bifaciality [5] make SHJ cells attractive for deployment in hot climates and regions with high albedos. Their low-temperature and rather simple manufacturing process (includes only four fabrication steps [6,7]) make them compatible with thin *c*-Si wafers. With all these benefits, the long-term outlook for SHJ solar cells appears very positive, as highlighted in recent ITRPV report [8].

One of the key factors that can limit the efficiency of SHJ solar cells is damage of ultra-thin *a*-Si:H layers and/or *a*-Si:H/*c*-Si interface during sputtering of transparent conductive oxide (TCO) layers. Despite sputter damage is known for decades the exact mechanism of this effect on SHJ solar cells is still not well understood. In many cases it is also not clear what is exactly being damaged: *a*-Si:H layers and/or *a*-Si:H/*c*-Si interface. Most researchers attribute sputter damage to the energetic ion bombardment [9,10], while some of them partly to the UV photon flux of the magnetron discharge [10–12] and others to the ion flux [13,14] or even phonons [15]. Obviously, the thicker *a*-Si:H layers, the less sputter damage. However, in high efficiency SHJ devices the doped and intrinsic layers must have the minimal thickness, particularly at the front surface facing the Sun, which exacerbates the problem of sputter damage.

In this study, we employed different buffer layers at the *a*-Si:H/*c*-Si interface in SHJ solar cells in order to get more insights into the underlying physics of sputter damage along with illuminated annealing (IA) for its recovery. Usually, the post-treatment of SHJ solar cells such as the IA at elevated temperatures can enhance the SHJ cell efficiency by $0.1-0.7\,\%_{abs.}$ [16–21], depending on the cell design and the IA conditions. Here, we demonstrate for the first time that the conversion efficiency of SHJ cells can be improved by more than $7.0\,\%_{abs.}$ by the IA at certain conditions. The paper is organized as follows. Differences in laboratory and industrial magnetron sputtering (often referred as to physical vapor deposition (PVD)) tools and mechanisms of sputter damage are briefly defined in Sec. 1. The experimental details are described in Sec. 2, followed by experimental results and discussion in Sec. 3. Conclusions are presented in the final section.

2. Magnetron sputtering sources and sputter damage

As mentioned above, sputter damage during the TCO deposition is commonly attributed to the bombardment of the substrate by a number of highly energetic charged particles. These particles have different fluxes and energies at the substrate surface, controlled by the electric potential

profile between the target and the substrate. The potential profile apart of the common plasma discharge parameters (gas pressure, discharge power) also depends on the excitation mode (RF, DC, pulsed DC or combined) and the magnetic field (B-field) design. Unfortunately, many authors do not specify what type of B-field profile is used in their studies. Nevertheless, it should be stressed that magnetic field plays an essential role in the performance of sputter magnetrons due to the electron confinement. In general, two major types of B-field profile can be found in planar magnetrons, balanced or unbalanced [22,23], as schematically shown in Figure 1.

In balanced magnetrons, all B-field lines are closed to the target resulting in plasma confinement within the magnetron plasma racetrack — a closed-loop B-field pattern (Figure 1, a). Therefore, the ion flux to the substrate surface is relatively small $< 1\,\text{mA/cm}^2$ ($< 10^{15}\,\text{ions/cm}^2 \cdot \text{s}$) [22]. In unbalanced magnetrons, some of B-field lines cross the substrate surface allowing electrons to escape from the racetrack region. These electrons then create less dense plasma away from the magnetron target surface, resulting in much higher ion flux to the substrate surface ($\leq 10^{16}\,\text{ions/cm}^2 \cdot \text{s}$) in comparison to balanced magnetrons (Figure 1, b). Both types of planar magnetrons are commonly used in laboratory magnetron sputtering tools, which employ relatively weak ferrite magnets. On the other hand, rotatable cylindrical magnetrons (Figure 2, b) — the workhorse of the PV industry mainly due to their high target utilization — employ balanced B-fields using strong rear-earth (neodymium or samarium-cobalt) magnets. Stronger B-fields confine electrons better, leading to denser plasma near the magnetron target surface and less ion flux to the substrate. Unlike laboratory magnetron sputtering tools, in industrial PVD tools the substrate holder (carrier) is always movable, resulting in excellent TCO film thickness uniformity. In the industrial manufacturing of SHJ solar cells, rotatable cylindrical magnetrons are exclusively powered by DC power supplies due to their stability, high deposition rates and simplicity, high production throughput.

In laboratory, magnetron sputtering discharges are mostly powered either by DC or RF (13.56 MHz) power supplies. Due to the different ionization mechanisms in DC and RF discharges, the electric potential profiles are quite different for these two excitation modes. DC discharges are based on the generation of ion-induced secondary electrons at the cathode (target) surface. Therefore, high negative target voltages are necessary to sustain the DC plasma because the electron emission increases almost linearly with the ion velocity [24].

On the other hand, RF plasmas are mainly driven by ionization due to electrons that perform an oscillating motion in the plasma volume since they can follow the RF frequency, unlike heavy ions. This kind of excitation is much more effective at low working pressures required for magnetron discharges (typically $\leq 10\,\text{mTorr}$) compared to the ionization by non-oscillating secondary electrons, leading to lower target voltages (also referred in the literature

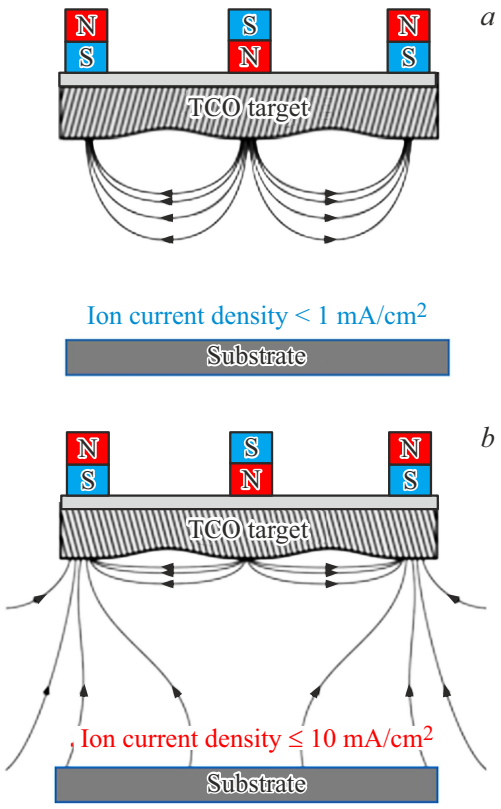

Figure 1. Magnetic field lines in (a) balanced and (b) unbalanced magnetron discharge.

as the DC bias) in RF discharges (Figure 2, a). However, the electron confinement in RF magnetron discharges is not as efficient as in DC discharges. This is because during the positive voltage half-cycle the target acts as anode (instead of cathode in the negative voltage half-cycle). Therefore, the plasma density in the front of the substrate is significantly higher for RF compared to DC excitation. Consequently, the positive ion flux (Ar^+, O^{2+}, O^+, In^+, Sn^+ in the case of ITO sputtering) at the substrate surface is higher in the case of RF excitation. However, its contribution to sputter damage is rather small due to low ion energy (10s eV) and, therefore, the positive ions can only affect a very thin subsurface of doped a-Si:H layers. On the contrary, some part of negative ions (mostly O^- [25]) formed near the target surface can be accelerated to relatively high energies (up to the DC bias) across the cathode sheath, which at low pressures can easily cross the distance between the target and the substrate without any energy loss. Due to this reason, O^- ions potentially can penetrate the doped a-Si:H layers deeper (particularly in DC magnetron discharges, in which the O^- ion energy and flux are higher [26]) and some researchers believe that they are the main reason of sputter damage in SHJ solar cells.

To our knowledge, there is no literature addressing the problem of O^- ion penetration in doped a-Si:H layers, particularly in such low energy range. However, there are

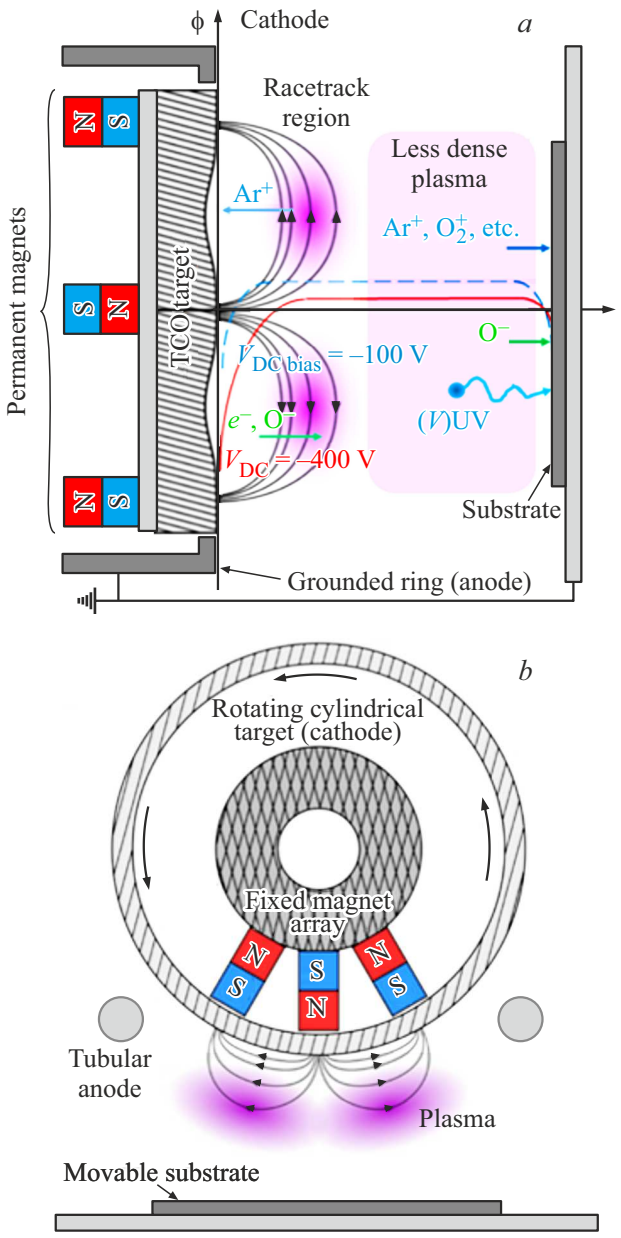

Figure 2. Schematic side-view of (*a*) planar magnetron discharge showing main sources of plasma damage and electric potential (ϕ) distributions in the case of DC (red solid line) and RF (blue dotted line) excitation under otherwise identical conditions [24] and (*b*) rotatable cylindrical magnetron discharge.

many studies on the Ar^+ ion incorporation in crystalline and hydrogenated amorphous silicon. For instance, in [27,28] it is shown that Ar^+ ions with an energy of 100–500 eV are stopped inside a 2-nm-thick *c*-Si layer. While SRIM (Stopping and Range of Ions in Matter) simulations, based on binary collisions [29,30], demonstrate a 20 nm and a 4 nm penetration depth for 5 keV and 300 eV Ar^+ ions in doped and intrinsic *a*-Si:H layers, respectively [31,32]. Studies on O^+ ion implantation for local oxide formation in Si [33] have shown that 4.5 keV O^+ ions (at fluences $\leq 10^{17}$ ions cm^{-2}) are mostly stopped within a 20-nm-thick sublayer. Taking into account the energy difference, it is reasonable to assume that all energetic negative ions (including O^-, etc.) during the ITO sputtering on Si hetero-structures are buried inside doped *a*-Si:H layers (typically having thicknesses ≥ 10 nm) in both DC and RF excitation modes. This assumption is also supported by recent results obtained in [15], which show a penetration depth about few nm for both O^- and electrons in *n*-type nanocrystalline silicon carbide (*n-nc*-SiC:H). In other words, energetic negative ions as well as electrons are not able to damage directly the *a*-Si:H/*c*-Si interface. Besides, the growing ITO layer relatively fast hinders their interaction even with doped and intrinsic *a*-Si:H layers.

If the energetic ions or electrons cannot reach the *a*-Si:H/*c*-Si interface, it is natural to ask what causes its damage. The answer could be energetic photons that are massless and have no electric charge hence could penetrate deeper in solids. Like the ion flux, the UV flux is directly proportional to the electron density. The reported vacuum UV (VUV, $\lambda < 200$ nm) fluxes in plasma discharges range from about 10^{14} to 10^{17} photons $cm^{-2} \cdot s^{-1}$ while the electron density ranges from 10^9 to 10^{12} cm^{-3} [34]. Therefore, in balanced magnetron sputtering discharges the VUV/UV flux to the substrate surface can actually exceed the ion flux due to the strong electron confinement, as described above. It should also be stressed however, that lower DC bias voltages in RF magnetron discharges lead to significantly lower deposition rates compared to DC sputtering processes under otherwise identical conditions (the same level of discharge power) [24,35]. Consequently, at the equal ITO layer thickness samples in RF magnetron discharges will be exposed to plasma longer compared to DC excitation, resulting in higher ion/photon fluences.

3. Experimental details

To investigate sputter damage, four types of bifacial SHJ cells with different buffer layers at the *a*-Si:H/*c*-Si interface were fabricated, as described below. To manufacture the SHJ cells, commercial-grade phosphor-doped wafers (CZ, ⟨100⟩, 156.75 × 156.75 mm) with a resistivity of 1.2–1.5 Ω · cm and a thickness of 150 μm were used. The cells featured the rear emitter design and were based on Si hetero-structures with identical intrinsic and doped layers, as schematically shown in Figure 3. Intrinsic (*i-a*-Si:H) and doped (*n-nc*-Si and *p-a*-Si:H) layers had the same thickness of 5 nm and 16 nm, respectively. Two types of buffer layers were employed: 1-nm-thick amorphous silicon carbide (*a*-SiC:H) and 5-nm-thick amorphous silicon (*a*-Si:H). Both buffer layers had high hydrogen content, i. e. were grown at high hydrogen dilution. Higher thickness of *a*-Si:H layers was chosen to examine the ion bombardment effect. Type A cells employed symmetric *a*-SiC:H buffer layers, Type B — front *a*-SiC:H and rear *a*-Si:H layers, Type C — reverse to Type B, Type D — similar to Type A,

but with symmetric *a*-Si:H layers, as shown in Figure 3. Five identical cells were processed for each type to ensure statistical significance of results.

After deposition of the buffer, intrinsic and doped layers by VHF-PECVD ($f = 40.68$ MHz, Oerlikon KAI-1200 reactors), the silicon hetero-structures were characterized by a Sinton Consulting WCT120 tool in the quasi-steady state mode [36] to determine the effective minority carrier lifetime (τ_{eff}) and the implied-V_{OC} at a minority charge carrier density of 10^{15} cm^{-3} and one sun illumination intensity, respectively. Then, indium tin oxide (ITO) layers with a thickness of 100 nm were deposited on both sides of the Si hetero-structures using an unbalanced planar magnetron source with a ceramic target ($In_2O_3/SnO_2 = 90/10$) powered by a RF ($f = 13.56$ MHz) power supply in a Plasmalab System 400 sputter coater (Oxford Instruments). The diameter of ITO target was 6 inches. To improve the ITO film thickness uniformity, the rotational movement of the substrate at a fixed rotation speed (2 rpm) and a restrictive mask were employed [37]. The distance between the target and the substrate was 90 mm. The RF power during ITO sputtering was 300 W, with a gas pressure of 5 mTorr and a substrate temperature of 25–30 °C.

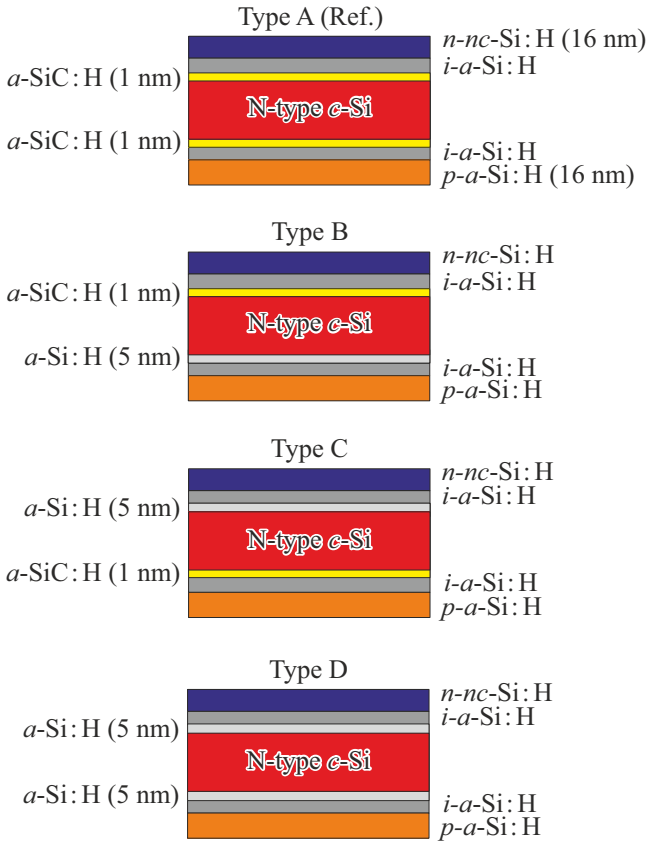

Figure 3. Cross-sectional drawings of the SHJ solar cells investigated herein. The surface texture, ITO layers and screen-printed Ag contact grids are not shown in the figure. (*n-nc*-Si:H — *n*-type hydrogenated nanocrystalline silicon, *a*-SiC:H — hydrogenated amorphous silicon carbide).

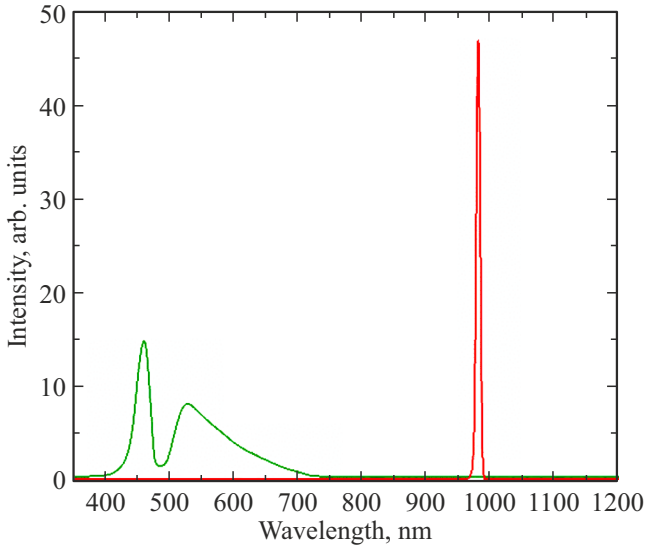

Figure 4. Emission spectrum of a white light-emitting diode and a near infrared laser.

The gas flow rates for argon and oxygen were 50 and 0.2 sccm, respectively. The thickness and optical properties of *a*-Si thin films and ITO layers were characterized by a spectroscopic ellipsometer (Horiba, Yobin Yvon).

Sputtering of ITO layers was followed by screen printing of the front and rear contact grids using a low-temperature Ag-based paste with subsequent curing. The SHJ solar cells were then illuminated using a distributed light source based on white LEDs, which was carefully calibrated to have an equivalent power density comparable to AM1.5 solar irradiance (1000 W/m^2) and a light uniformity over 200×200 mm^2 illumination area below 5 %. The emission spectrum of white LEDs is shown in Figure 4. During 10 min illumination of the front side (*n-nc*-Si:H), the cell temperature was maintained at 200 °C. The one sun current-voltage (I-V) measurements were taken using a solar simulator under standard testing conditions before and after the IA.

4. Results and discussion

To confirm that the PVD processes cause the cell damage, the effective lifetime measurements were taken first. Table 1 shows that type A cells with symmetric *a*-SiC:H buffer layers have the highest values of effective lifetime (τ_{eff}) and implied-V_{OC}. The replacement of *a*-SiC:H buffer layer by *a*-Si:H either on the rear (emitter) (type B cells) or front (type C cells) side results in a moderate reduction of both τ_{eff} and implied-V_{OC}. Obviously, the reduction is stronger for the emitter side due to poorer passivation properties of *a*-Si:H buffer layer. The worst case is observed for type D cells having *a*-Si:H buffer layers on both sides.

Figure 5 shows a comparison of the I-V characteristics of the complete SHJ solar cells before and after illuminated

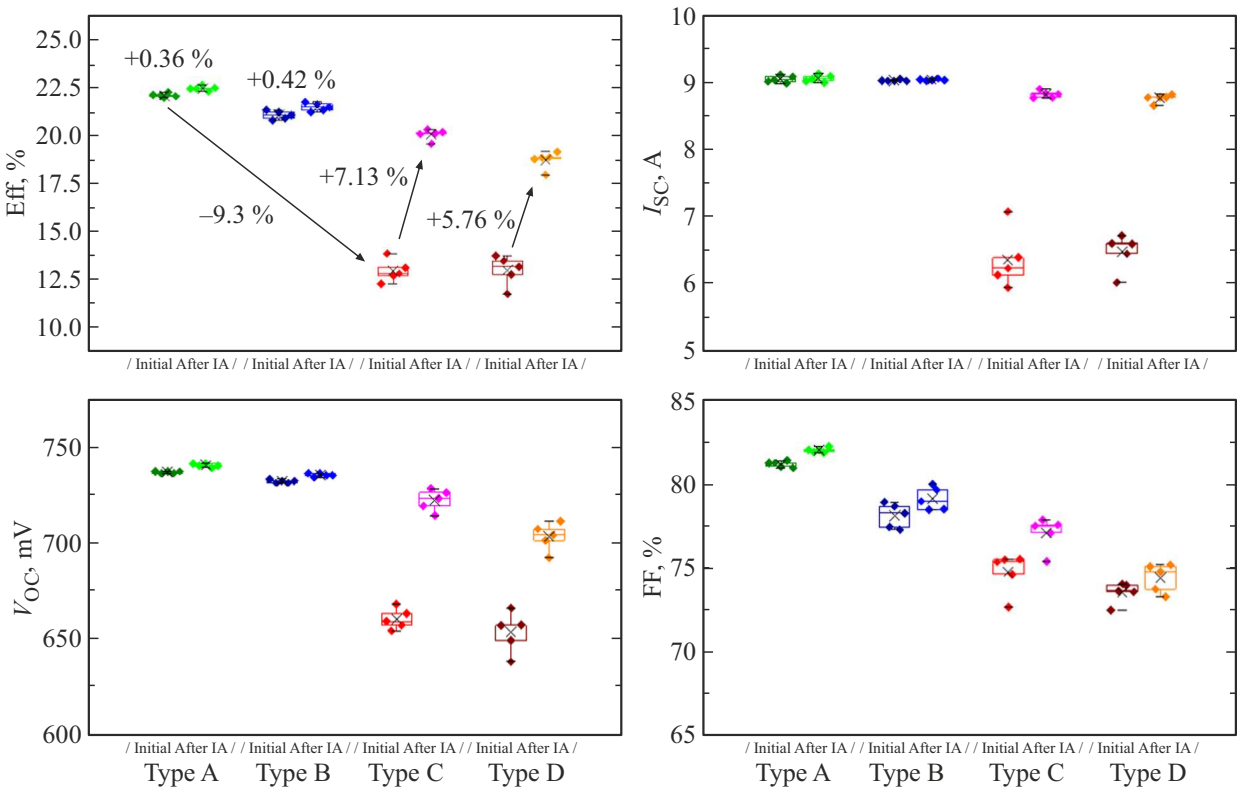

Figure 5. Current-voltage characteristics of the SHJ solar cells before and after the illuminated annealing.

annealing (1 Sun, 200 °C, 10 min). It is seen that before the IA type A and type B cells exhibit the open circuit voltages (V_{OC}) that are slightly below or comparable to their implied-V_{OC}, which is typical for SHJ solar cells. Damage processes at the ITO/doped layer interfaces most likely cause such small sputter damage, as explained below. The short-circuit current (I_{SC}) of type A and type B cells is not changed, while V_{OC} and fill factor (FF) are slightly improved by the IA. The improvement in V_{OC} (+3 mV) and FF (+0.12–0.14 %) leads to an average efficiency gain of 0.36 % and 0.42 %$_{abs.}$, respectively, which are typical values for the IA process. Higher efficiency gains (up to 0.7 %$_{abs}$) can be obtained when intense NIR laser beams (Figure 4) are used as the light source [18,20,21]. This might be attributed to better annealing of the ITO layers due to their higher absorption in the NIR range [38] compared to the visible range in the case of white LEDs. Annealing of the ITO layers is also inline with a reduction of the series resistance of SHJ cells by the IA observed in [21].

On the contrary, for type C and type D cells there is a strong deviation of V_{OC} (loss of more than 70 mV) from the initial implied-V_{OC}, as can be seen in Figure 5 and Table 1. In fact, these cells exhibit significant decrease of all parameters in comparison with type A and type B cells. For example, the conversion efficiency of type C and type D cells is less by more than 9 %$_{abs.}$ compared to the type A cells. Nevertheless, the IA essentially recovers the anomalous sputter damage, as illustrated in Figure 5.

However, for type C and type D cells the V_{OC} after the IA are still below the initial implied-V_{OC} (Table 1). Obviously, the ion bombardment cannot explain such

Table 1. Parameters of silicon heterostructures used in this study

Cell type	ρ (Ω cm)	τ_{eff} (μs)	implied V_{OC} (mV)
Type A	1.33	2018	740
	1.32	1668	738
	1.45	1996	739
	1.19	1831	739
	1.28	1660	738
Type B	1.47	1255	730
	1.43	1116	730
	1.44	1157	730
	1.49	1163	729
	1.29	999	729
Type C	1.48	1745	735
	1.30	1609	735
	1.44	1774	736
	1.28	1598	735
	1.45	1777	736
Type D	1.32	902	726
	1.45	1090	729
	1.40	1011	728
	1.23	872	726
	1.43	1136	729

Table 2. Common bonds in hydrogenated silicon and silicon carbide and their energies [37]

Bond	Energy, eV
Si-Si	2.34
Si-H	3.34
C-H	4.60
Si-C	3.21
C-C	3.70
H-H	4.48

anomalous sputter damage because the *a*-Si:H buffer layer is 5 times thicker the *a*-SiC:H layer and due to arguments described in Sec. 2. The phonon scenario proposed in [15] is also questionable in this case, however phonons may play an essential role in the IA, as explained at the end of this section.

Interestingly, anomalous sputter damage appears only when the *a*-Si:H buffer layer is located under the *n-nc*-Si:H layer (type C/D cells in Figure 3). However, when the buffer layer is replaced by *a*-SiC:H (type A/B cells) the sputter damage is minimal. To explain this fact let us look at Figure 6, in which the absorption coefficients of various *a*-Si layers are shown. It is clear that *n-nc*-Si:H layer with a thickness of 16 nm absorbs all UV photons with energies above 3.5 eV, whereas *p-a*-Si:H layer with the same thickness transmits only photons with energies below 3.2 eV. On the other hand, it is well known that the high *H*-content *a*-Si:H and *a*-SiC:H films usually contain a large number of Si-H and C-H bonds [39], respectively. Si-H bonds are commonly attributed to the surface passivation quality and the formation of dangling bonds that behave as defects and recombination centers. The Si-H bond energy is 3.34 eV, as shown in Table 2. Figure 6 shows that *p-a*-Si:H layer blocks all photons that are capable to break Si-H bonds at the *a*-Si:H/*c*-Si interface. However, this is not the case for *n-nc*-Si:H that transmits photons with energies ≤ 3.5 eV. Higher energy (≥ 4.6 eV) is required to break C-H bonds, however such energetic UV photons are well absorbed by both *n-nc*-Si:H and *p-a*-Si:H layers. This explains why type A/B cells have minimal UV damage, unlike type C/D cells.

As mentioned above (Sec. 2), during ITO deposition both positively and negatively charged particles cannot reach the *a*-Si:H/*c*-Si interface. They all are stopped in the near-surface region of doped layers with a thickness of few nm.

Nevertheless, they can create additional defects at the interface with ITO layers. For example, assuming an Ar ion flux of $10^{15}-10^{16}$ ions/cm$^2\cdot$ s, an ion penetration depth of 5 nm and an ITO deposition rate of 10 nm/s one can roughly estimate the averaged Ar ion concentration in the near-surface region of $10^{21}-10^{22}$ cm^{-3} that is comparable with

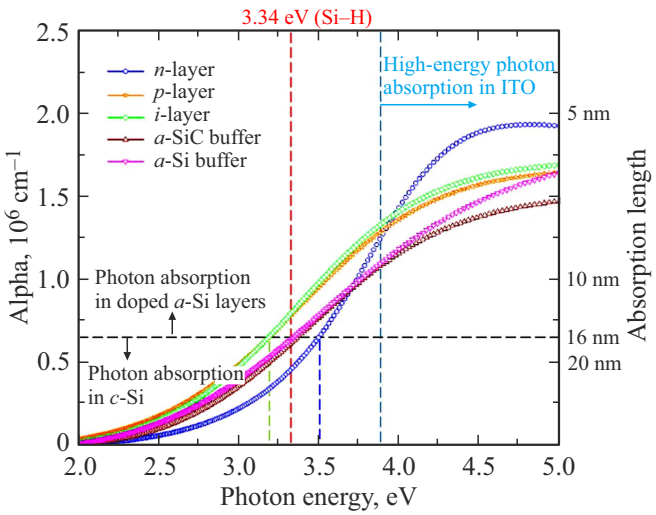

Figure 6. The absorption coefficient of various layers employed in the SHJ solar cells as a function of the photon energy.

the doping level of *n*-layer. On the other hand, relatively energetic ions can lead to sputtering (displacement) of Si and/or H atoms. At the normal incidence of Ar^+ over the *c*-Si surface, the threshold energy for sputtering is approximately 40 eV [40]. Once the sputtering event is happened, the surface structure is strongly deformed, and thus the additional surface defects are generated. These defects are likely represent the part of sputter damage that cannot be recovered within short (few seconds) time scales by the dark or illuminated (1 Sun) annealing at elevated temperatures.

To minimize such defects the *B*-field should be strong and balanced and the deposition rate of ITO layers should be maximal, which is usually achieved in industrial PVD tools, in which a high throughput ($>$ 4000 cells/h [41]) is necessary. This means that commercial SHJ cells are exposed to the DC magnetron discharge powered by a kW-range DC power supply on a time scale of few seconds. For the effective IA at elevated temperature within such short time scale the light intensity should be increased up to 100 Suns [21]. On the contrary, in laboratory PVD tools the deposition rate is often limited, particularly in those equipped with RF power supplies, in which the deposition time can reach few minutes. In this study, the ITO (100 nm) deposition time was 83 s, resulting in higher ion/photon fluences. Nevertheless, the IA for 10 min at 1 Sun (white LEDs) and 200 °C is sufficient for annealing defects at the ITO/doped layer interface, as demonstrated by type A/B cells (V_{OC} $>$ implied-V_{OC} after the IA).

Unlike the ions, the growing ITO layer decreases the UV flux ($<$ 400 nm) at lower rate, as demonstrated in Figure 7. For example, it is seen that ITO layers with a thickness of 20 nm still transmit 25 % of 6.2 eV photons ($\lambda = 200$ nm) and about 50 % of 4.1 eV photons ($\lambda = 300$ nm). Obviously, UV photons with energies above 6 eV (VUV) can only interact with doped and intrinsic *a*-Si:H layers at the very

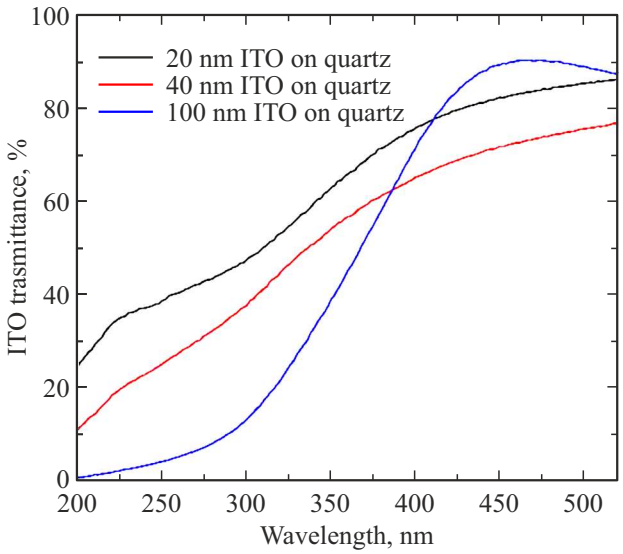

Figure 7. The optical transmittance of ITO films with different thickness grown on fused quartz substrates by the RF magnetron discharge as a function of the optical wavelength.

beginning of the growth process. When the ITO layer growth is completed and the required thickness of 100 nm is reached, ITO can only transmit 10 % of 4.1 eV photons due to its relatively high bandgap energy, as shown in Figure 7.

In our case, VUV photons are effectively absorbed by doped layers (Figure 6) and do not reach the *a*-Si:H/*c*-Si interface. However, higher bandgap doped layers such as nanocrystalline silicon carbide with a thickness above 10 nm may transmit some part of VUV photons [42] and damage the interface. This may explain experimental results obtained in [15] rather than the energy transfer to the *c*-Si interface via phonons. It should be stressed that bond breaking is an endothermic process and sufficient energy is required to break the chemical bonds, as shown in Table II. On the contrary, phonons are usually considered as quantized sound waves hence they have energies typically below 0.1 eV, i. e. more than an order of magnitude smaller the energy of UV photons that travel at the speed of light. On the other hand, bond making is always an exothermic process and energy is transferred to the solid as the new bonds are formed, supporting the fact that the recovery of Si-H bonds can happen even at room temperature. Extra energy (heat or light) in this case only accelerates the process (due to H diffusion to dangling bonds). Therefore, phonons that play an essential role in heat transfer are more appropriate for the description of dark/illuminated annealing rather than sputter damage.

5. Conclusions

Various mechanisms of sputter damage in SHJ solar cells have been examined. It is shown that energetic charged particles can damage only the ITO/doped layer interface. Therefore, damage of the *a*-Si:H/*c*-Si interface by energetic positive and/or negative ions is a myth, unless the total thickness of doped/intrinsic *a*-Si:H layer stack is below 5 nm. Illuminated annealing at elevated temperature is effective in annealing defects at the ITO/doped layer interface. To mitigate such damage, the magnetron discharge should be balanced with a strong magnetic field and operate in the DC mode at the maximum deposition rate. These requirements are satisfied in industrial PVD tools, but are rarely achieved in laboratory magnetron sputtering systems.

It is revealed that if the doped/intrinsic *a*-Si:H layers are transparent to UV photons then the *a*-Si:H/*c*-Si interface can directly be damaged, resulting in severe degradation of the SHJ cell performance. The IA at elevated temperature can recover most of such damage. The use of silicon carbide buffer layer at the *a*-Si:H/*c*-Si interface helps to suppress the NUV photon damage. Among DC and RF magnetron discharges, unbalanced RF magnetron discharges result in the highest UV photon damage under otherwise identical discharge conditions.

Conflict of interest

The authors declare that they have no conflict of interest.

References

[1] H. Lin, *et al.*. Nat. Energy, **8**, 789 (2023).
[2] X. Ru, *et al.*. Joule, **8** (4), 1092 (2024).
[3] M. Taguchi, E. Maruyama, M. Tanaka. Jap. J. Appl. Phys., **47**, 814 (2008).
[4] A.V. Sachenko, *et al.*. J. Appl. Phys., **119**, 225702 (2016).
[5] I. Romijn. „Bifacial solar cells — a brief review“, presented at nPV workshop (Konstanz, Germany, 2017).
[6] C. Ballif, S. De Wolf, A. Descoeudres, Z.C. Holman. Semiconductors and Semimetals, **90**, 73 (2014).
[7] A.S. Abramov, D.A. Andronikov, S.N. Abolmasov, E.I. Terukov. *Silicon Heterojunction Technology: A Key to High Efficiency Solar Cells at Low Cost, in High-Efficiency Low-Cost Photovoltaics: Recent Developments*, V. Petrova-Koch, R. Hezel, and A. Goetzberger, Eds. (Cham: Springer International Publishing, 2020) pp. 113-132.
[8] ITRPV, International Technology Roadmap for Photovoltaic, 15th Ed., May 2024.
[9] E. Aydin, *et al.*. Matter, **4** (11), 3549 (2021).
[10] B. Demaurex, S. De Wolf, A. Descoeudres, Z.C. Holman, C. Ballif. Appl. Phys. Lett., **101**, 171604 (2012).
[11] B.M. Meiners, S. Holinski, P. Schäfer, S. Hohage, D. Borchert. Proc. 31th European PV Solar Energy Conference (14-18 September, Hamburg, Germany, 2015).
[12] V. Linss, M. Bivour, H. Itawa, K. Ortner. 9th International Conference on Crystalline Silicon Photovoltaics, AIP Conf. Proc., **2174**, 040009 (2019).
[13] A. Illiberi, P. Kudlacek, A.H.M. Smets, M. Creatore, M.C.M. van de Sanden. Appl. Phys. Lett., **98**, 242115 (2011).
[14] A.H.T. Le, V.A. Dao, D.P. Pham, S. Kim, S. Dutta, C.P.T. Nguyen, Y. Lee, Y. Kim, J. Yi. Sol. Energy Mater. Sol. Cell., **192**, 36 (2019).
[15] A. Eberst, *et al.*. Adv. Phys. Res., 2400036 (2024).

[16] E. Kobayashi, *et al.*. Appl. Phys. Lett., **109**, 153503 (2016).
[17] E. Kobayashi, *et al.*. Sol. Energy Mater. Sol. Cell., **173**, 43 (2017).
[18] M. Wright, M. Kim, P. Dexiang, Z. Wenbin, B. Wright, B. Hallam. AIP Conf. Proc., **2147**, 110006 (2019).
[19] C. Madumelu, B. Wright, A. Soeriyadi, M. Wright, D. Chen, B. Hoex, B. Hallam. Sol. Energy Mater. Sol. Cell., **218**, 110752 (2020).
[20] M. Wright, A. Soeriyadi, B. Wright, D. Andronikov, I. Nyapshaev, S. Abolmasov, A. Abramov, B. Hallam. IEEE J. Photovoltaics, **12**, 267 (2022).
[21] M. Wright, *et. al.*. A.H. Soeriyadi, M. Kim, B. Wright, B.V. Stefani, D. Andronikov, I. Nyapshaev, S. Abolmasov, A. Abramov, R.S. Bonilla, B. Hallam. Sol. Energy Mater. Sol. Cell., **248**, 112039 (2022).
[22] S.N. Abolmasov. Plasma Sources Sci. Technol., **21**, 035006 (2012).
[23] J.T. Gudmundsson. Plasma Sources Sci. Technol., **29**, 113001 (2020).
[24] K. Ellmer,J. Phys. D: Appl. Phys., **33**, R17 (2000).
[25] T. Welzel, K. Ellmer. J. Vac. Sci. Technol. A, **30**, 061306 (2012).
[26] Welzel, K. Ellmer. J. Phys. D: Appl. Phys., **46**, 315202 (2013).
[27] W.M. Lau, I. Bello, L.J. Huang, X. Feng, M. Vos, I.V. Mitchell. J. Appl. Phys., **74** (12), 7101 (1993).
[28] M.C. Moore, N. Kalyanasundaram, J.B. Freund, H.T. Johnson. Nuclear Instruments and Methods in Physics Research B, **225**, 241 (2004).
[29] P. Sigmund. Phys. Rev., **184**, 383 (1969).
[30] R. Behrisch (ed.). Sputtering by Particle Bombardment I, II and III, Top. Appl. Phys., **47**, **52**, **64** (Springer, Berlin, Heidelberg 1981, 1983, 1991), Russ. Translation: (MIR, Moscow 1984, 1 986, 1998).
[31] A. Defresne, O. Plantevin, P. Roca i Cabbarocas. AIP Advances,**6**, 125107 (2016).
[32] S. Nunomura, T. Tsutsumi, K. Nakane, A. Sato, I. Sakata, M. Hori. Jap. J. Appl. Phys., **61**, 056003 (2022).
[33] D. Krüger, R. Kurps, P. Formanek, G. Weidner. Solid State Phenomena, **95-96**, 77 (2003).
[34] D. Popović, M. Mozetičx, A. Vesel, G. Primc, R. Zaplotnik. Plasma Processes and Polymers, e2100061 (2021).
[35] F. Kurdesau, G. Khripunov, A.F. da Cunha, M. Kaelin, A.N. Tiwari. Journal of Non-Crystalline Solids, **352** (9-20), 1466 (2006).
[36] R.A. Sinton, A. Cuevas, M. Struckings. Proc. 25th Photovoltaic Specialists Conference (Washington DC, USA, 1996) pp. 457-460.
[37] I.A. Starkov, I.A. Nyapshaev, A.S. Starkov, S.N. Abolmasov, A.S. Abramov, V.S. Levitskiy, E.I. Terukov. J. Vac. Sci. Technol. A, **35** (6), 061301 (2017).
[38] P. Lippens, D. Chiu, C. Szepesi. Proc. 27th European Photovoltaic Solar Energy Conference and Exhibition (Frankfurt, Germany, 2012) pp. 2079-2082.
[39] H. Efstathiadis, Z. Yin, F.W. Smith. Phys. Rev. B, **46**, 13119 (1992).
[40] K. Wittmaack. Phys. Rev. B, **68**, 235211 (2003).
[41] S.K. Chunduri, M. Schmela. „Heterojunction Solar Technology: working hard on cost reductions“, TaiyangNews Report, 2023.
[42] T. Chen, F. Köhler, A. Heidt, R. Carius, F. Finger. Proc. 39th Photovoltaic Specialists Conference (Tampa, FL, USA, 2013) pp. 0917-0920.